Research Paper

Journal of Engineering and Technological Sciences

Investigation of Reaction Dynamics of Methane Reforming on Nickel Clusters Using Molecular Dynamics Simulations

Rizal Arifin[1],*, Fikrun Najib Muzakki[1], Yoyok Winardi[1], Ida Widaningrum[1], Zulkarnain[2], Abdurrouf[3], Norhasnidawani Johari[4], Vannajan Sanghiran Lee[5] & Darminto[6]

[1]Faculty of Engineering, Universitas Muhammadiyah Ponorogo, Jalan Budi Utomo No. 10, Ponorogo 63471, Indonesia
[2]Department of Physics Education, Universitas Muhammadiyah Mataram, Jalan KH Ahmad Dahlan No. 1, Mataram 83127, Indonesia
[3]Department of Physics, Brawijaya University, Jalan Veteran, Malang 65145, Indonesia
[4]Malaysia-Japan International Institute of Technology, Universiti Teknologi Malaysia, Jalan Sultan Yahya Petra, Kuala Lumpur 54100, Malaysia
[5]Centre of Excellence in Quantum Information Science and Technology (QIST), Department of Chemistry, Faculty of Science, Universiti Malaya, 50603, Kuala Lumpur, Malaysia
[6]Department of Physics, Institut Teknologi Sepuluh Nopember, Kampus ITS Sukolilo, Surabaya 60111, Indonesia

*Corresponding author: rarifin@umpo.ac.id

Abstract

This study employed molecular dynamics simulations utilizing the ReaxFF force field to elucidate the mechanisms underlying methane decomposition and hydrogen generation on nickel clusters (Ni_{37}, Ni_{55}, and Ni_{80}). The transformation of methane into valuable products, including carbon species and hydrogen molecules, is of considerable significance owing to the abundance of methane and its potential role as an atmospheric pollutant. The findings suggest that Ni_{37} clusters had the highest initial reactivity, although they deactivated swiftly; conversely, Ni_{55} and Ni_{80} exhibited more consistent reaction rates. The highest efficiency of hydrogen production per unit surface area was displayed by Ni_{55} clusters within 100,000 fs, demonstrating a balance between reactivity and stability. Methane dissociation on the Ni55 clusters occurred in multiple stages. Two distinct mechanisms for hydrogen formation were identified: simultaneous dissociation from methane and migration and the combination of hydrogen atoms on the cluster surface. Ni_{55} showed a substantially lower activation energy for methane dissociation at 0.5 eV than bulk nickel, suggesting a higher degree of reactivity. Conversely, the activation energy for hydrogen formation was 1.1 eV. These results highlight the potential of the Ni_{55} clusters as effective catalysts for hydrogen production and methane conversion.

Keywords: *activation energy; catalysis; hydrogen generation; methane decomposition; molecular dynamics; nickel cluster; ReaxFF force field.*

Introduction

Methane (CH_4) is a potent greenhouse gas and a major environmental contaminant. The global oil and natural gas industry is a significant contributor to CH_4 emissions, releasing gas through leakage, incomplete combustion, flaring, and venting in various processes (Roshchanka & Evans, 2014). Environmental pollution is exacerbated by direct emissions of this gas, which exhibits a greenhouse effect 20–30 fold greater than that of carbon dioxide (Lu, 2021). CH_4 emissions from sources such as landfills can lead to groundwater and air pollution, which can negatively impact climate and pose health hazards (Aljaradin, 2012). Although CH_4 is not directly toxic to humans, it is frequently co-emitted with other pollutants that can negatively affect adjacent communities, thus underscoring environmental justice concerns (Casey et al., 2021). Addressing systematic breaches in gas compressor units and pipelines is essential for reducing CH_4 emissions and their impact on the environment and nature (Strizhenok & Korelskiy, 2019). The conversion of CH_4 to hydrogen (H_2) molecules without the formation of greenhouse gases is highly advantageous, particularly because natural gas is predominantly composed of CH_4. By minimizing the overall generation of greenhouse gases, this process addresses environmental concerns and provides an alternative energy source (Kikuchi, 2002).

ISSN: 2337-5779
J. Eng. Technol. Sci. Vol. 57, No. 1, 2025,66-77
DOI: 10.5614/j.eng.technol.sci.2025.57.1.5

DOI: 10.5614/j.eng.technol.sci.2025.57.1.5

Several studies have emphasized the potential of catalytic methane decomposition (CMD) as a viable approach for the production of H_2 along with solid carbon or carbon nanostructures (Gamal et al., 2021; Harbin et al., 2023; Shelepova et al., 2022; Sun, 2024). This process is environmentally friendly and produces CO_x-free H_2 and solid carbon products (Dipu, 2021; Harbin et al., 2023). These materials have various applications in catalysis, electronics, and fuel cells (Gamal et al. 2021). CH_4 decomposition is widely acknowledged as a reliable method for producing H_2, offering a simpler and potentially more cost-effective alternative to steam reforming, as highlighted in recent studies (Hasnan et al., 2020; Rad et al., 2022). Furthermore, researchers have found that the thermal decomposition of CH_4 is promising for large-scale production of H_2. This process can mitigate the release of greenhouse gases, as noted by Sanchez-Bastardo et al. (2021) and Santos et al. (2022) and Hasnan et al. (2023). Researchers have investigated the use of different catalysts, including Cr–O–Ni and Ni-based perovskites, to enhance the production of H_2 and carbon nanotubes during CH_4 decomposition (Harbin et al., 2023; Sun, 2024). In addition, researchers have studied the catalytic decomposition of CH_4 under various conditions, such as the production of H_2 using nanomaterials (Fujimoto & Ohba, 2022). Arifin et al. examined the processes of CH_4 dehydrogenation and H_2 formation on Pt(100) (Arifin & Darminto, 2023) and Pt_7-Ni(110) (Arifin et al., 2024) surfaces, emphasizing the significance of metal surfaces in promoting the separation of hydrogen atoms from CH_4 molecules (Arifin et al., 2024; Arifin & Darminto, 2023). In addition, Arifin et al. (2015) performed first-principles calculations to gain insight into the process of CH_4 decomposition on a Ni(111) surface, providing valuable information on the fundamental aspects of CH_4 decomposition on metal catalysts. The above-mentioned studies highlight the potential of CH_4 decomposition as a sustainable and effective method for H_2 production. In the field of computational catalysis, numerous studies have utilized density functional theory (DFT) to investigate reaction mechanisms and catalyst characteristics. For instance, DFT has been applied to elucidate persulfate-based advanced oxidation processes and mechanisms of organic compound isomerization (Gallego-Villada et al., 2024; Zhang et al., 2021).

Nickel plays a vital role as a catalyst in CH_4 decomposition and H_2 formation owing to its exceptional catalytic properties. Furthermore, numerous studies have emphasized the importance of nickel-based catalysts in facilitating CH_4 decomposition reactions for H_2 production. For example, Chen and Lua employed electroless plating to create nickel catalysts for H_2 generation via CH_4 decomposition (Chen & Lua, 2020). In a recent study, Phichairatanaphong et al. successfully created a catalyst using nickel-supported mesoporous silica–aluminosilicate to improve H_2 production through CH_4 decomposition (Phichairatanaphong et al., 2021). Recently, Yan et al. examined the process of generating CO_x-free H_2 and graphene nanoplatelets via CH_4 decomposition using Ni-lignin-derived nanoparticles, placing particular emphasis on the role of nickel in the CH_4 decomposition process (Yan et al. 2022). In addition, previous studies have indicated that the addition of metals such as copper and iron to nickel-based catalysts can improve their catalytic activity in CH_4 decomposition reactions. Recently, Hasnan et al. prepared bimetallic nickel catalysts supported on mesostructured silica nanoparticles with copper and iron, which exhibited enhanced activity and stability for CH_4 decomposition (Hasnan et al., 2023). In another recent study, Vlaskin emphasized the effectiveness of using a Ni catalyst to enhance the efficiency of CH_4 decomposition by reducing the required temperature (Vlaskin, 2023). In addition, the size and dispersion of nickel particles are important factors in catalytic reactions. Recently, Liang et al. found that the deactivation rate of nickel catalysts in CH_4 decomposition was influenced by the size of nickel particles (Liang et al., 2020). Further, Wang et al. examined a pre-coking strategy that demonstrated the significance of nickel in catalytic processes; their findings highlighted how this strategy can improve the stability performance of supported nickel catalysts in hydrogenation reactions (Wang et al., 2021).

Extensive research has been conducted on metallic nickel catalysts, owing to their well-established high catalytic activity for CH_4 decomposition (Wang & Lua, 2012). However, recent studies have questioned the involvement of Ni clusters in this process (Harrath et al., 2023). Thus, further investigation is necessary to elucidate the specific mechanisms through which nickel clusters facilitate CH_4 decomposition and to provide insights into the fundamental processes at the nanoscale level. This study aimed to examine the molecular mechanisms and kinetics involved in the catalytic conversion of CH_4 over nickel catalysts. The objective of this study is to elucidate the dynamic mechanism of nickel clusters in the conversion of CH_4 to various products, including H_2, using molecular dynamics (MD) simulations. Thus, the current investigation aimed to clarify the precise interactions, dynamics, and energetics of CH_4 molecules in the presence of Ni surfaces, particularly in the context of reforming processes.

Methods

In this study, we used MD simulations to explore the reaction mechanisms of CH_4 on nickel clusters. Using the ReaxFF reactive force field, chemical reactions were dynamically modeled by adjusting the bond orders throughout the simulations (van Duin et al., 2001). This capability makes ReaxFF notably well suited for studying systems where chemical reactions are critical, such as those involving catalysis and combustion (van Duin et al., 2001). In this study, we optimized the ReaxFF potential parameters to accurately capture the interactions between CH_4 molecules and nickel clusters in hydrocarbon–metal systems (Mueller et al., 2010).

The simulation system included nickel clusters of various sizes (Ni_{37}, Ni_{55}, and Ni_{80}) surrounded by CH_4 molecules at a density of 0.58 g/mL. Different cluster sizes were selected to investigate their effects on the reaction mechanism and kinetics. The initial configurations of the Ni_{37}, Ni_{55}, and Ni_{80} clusters were obtained from the Cambridge Cluster Database and selected based on their structures in the lowest energy states, as determined by the Sutton-Chen potential (P. K. Doye & J. Wales, 1998). The simulations were conducted using the ReaxFF 2024.1 software package (Chenoweth et al., 2008; van Duin et al., n.d., 2001), which offers reliable tools for configuring and executing MD simulations with the ReaxFF force field.

The simulations were conducted over 100 ps, with a timestep of 0.25 fs for each run, which allowed the capture of fast reaction events and observation of the intricate dynamics of the systems. A Nosé–Hoover thermostat was employed to ensure temperature control and maintain a constant temperature for the systems throughout the simulations. The systems comprising Ni_{55} clusters were simulated at three temperatures: 1,400 K, 1,500 K and 1,600 K. Temperatures of 1400, 1500, and 1600 K were chosen for comparison with previous studies that employed 1500 K (Arifin et al., 2015) to investigate CH_4 reforming.

After the simulations, Ovito (Stukowski, 2009) was used to compute the average surface area of nickel clusters. This is crucial for gaining insight into the reactive surface area required for CH_4 dissociation and subsequent reactions. The activation energies of the reactions were calculated using the Arrhenius equation, as given by Eq. (1).

$$k = Ae^{-\frac{E_a}{RT}} \tag{1}$$

where k is the reaction rate constant, A is the pre-exponential factor, E_a is the activation energy, R is the universal gas constant (8.314 J/mol·K), and T is the temperature (K).

From an analysis of the reaction rates at various temperatures, we plotted the natural logarithm of the reaction rate constant, $\ln(k)$, against the reciprocal of the temperature, $1/T$. The slope of this plot, $-\frac{E_a}{R}$, was then used to determine the activation energy for CH_4 dissociation and H_2 molecule generation.

Results

This section provides results of the simulation, focusing on the mechanisms and efficiencies of CH_4 decomposition and H_2 generation on nickel clusters. First, the impact of the nickel cluster size (Ni_{37}, Ni_{55}, and Ni_{80}) on the rate of CH_4 decomposition and subsequent generation of H_2 were investigated. Second, the dynamics and reaction mechanisms of the Ni_{55} cluster were explored, including an examination of the temperature effects and detailed analysis of the simulated atomic interactions.

Effect of Nanocluster Size on CH_4 Decomposition and H_2 Generation

This subsection examines the effects of the nanocluster size on the rate of CH_4 decomposition and H_2 generation. Understanding these size-dependent effects is crucial for maximizing catalytic performance and advancing the development of nanostructured materials for efficient CH_4 conversion and H_2 production.

DOI: 10.5614/j.eng.technol.sci.2025.57.1.5

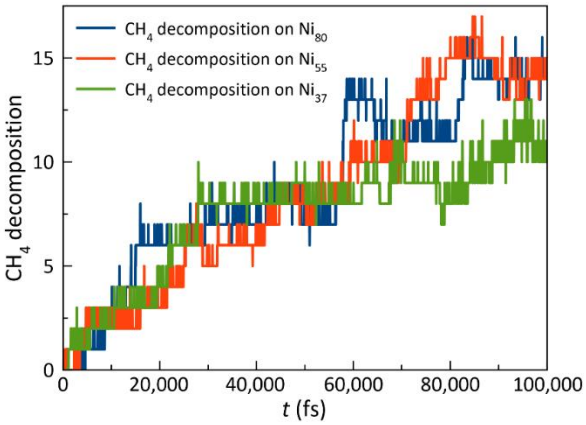

Figure 1 Number of dissociated CH_4 molecules on the surfaces of the Ni_{37}, Ni_{55}, and Ni_{80} clusters over 100,000 fs at T = 1,500 K.

Figure 1 illustrates the dynamic changes in the number of CH_4 decomposition events on the surfaces of Ni_{37}, Ni_{55}, and Ni_{80} clusters at T = 1,500 K. The initial dissociation of CH_4 was observed in the Ni_{37} system, followed by that in the Ni_{55} and Ni_{80} systems. Based on the observed trend, the reactivity of nickel nanoclusters decreased as their size increased. Thus, smaller clusters demonstrate a greater initial reactivity. The initial reactivity of the Ni_{37} clusters was assessed based on the early dissociation of CH_4 observed in the simulations. Although this offers a qualitative evaluation, further catalytic activity measurements, including turnover frequency (TOF), will be performed in subsequent studies to enable a quantitative comparison and enhance the understanding of catalytic performance across various cluster sizes. Nevertheless, the Ni_{37} catalyst exhibited a higher rate of deactivation than those of the Ni_{55} and Ni_{80} catalysts. The reaction rate of the Ni_{37} catalyst significantly decreased after approximately 30,000 fs. In addition, the total number of decomposed CH_4 molecules on the Ni_{37} surface after 100,000 fs was lower than those for the larger Ni_{55} and Ni_{80} catalysts.

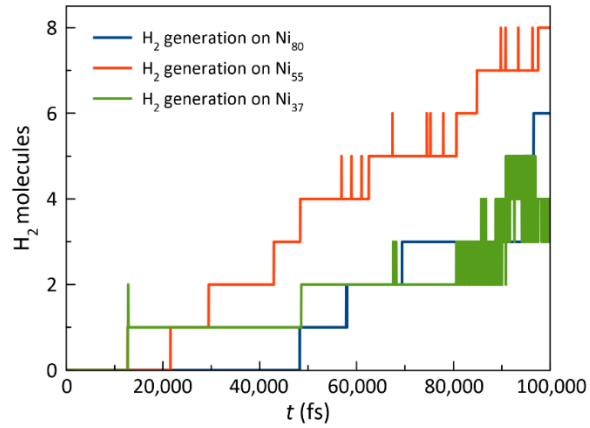

Figure 2 Number of H_2 molecules produced on the surfaces of the Ni_{37}, Ni_{55}, and Ni_{80} clusters over 100,000 fs at T = 1,500 K.

The formation of H_2 molecules exhibited a pattern comparable to that of the CH_4 decomposition process (see Figure 2), with Ni_{37} yielding the highest rate of H_2 production, followed by Ni_{55} and Ni_{80}. This suggests that smaller nickel clusters initially facilitate more rapid H_2 production because of their higher reactivity. Nevertheless, a notable observation is that the Ni_{55} system generates a greater number of H_2 molecules compared to the Ni_{37} system within 100,000 fs at a temperature of 1,500 K.

Furthermore, the dynamics of H_2 formation over time indicated that the reaction rates for the Ni_{55} and Ni_{80} clusters were comparable (as indicated by the slope of the graph, which represents the number of molecules produced per unit time). This indicates that although Ni_{80} may exhibit a slightly lower initial reactivity, its sustained performance over time is comparable to that of Ni_{55}. Within the time frame of 100,000 fs, the increased total H_2 yield of the Ni_{55} system highlights the potential of this cluster size for efficient H_2 production. These findings underscore the need for additional evaluations and longer simulation times to gain a comprehensive understanding of the long-term catalytic performance and stability of nickel clusters of various sizes. Although Ni_{37} and other smaller clusters may provide rapid initial reaction rates, their rapid deactivation requires a balance between their durability and reactivity. In this regard, Ni_{55} may represent the optimal size for harmonizing these factors, because it exhibits both high reactivity and sustained catalytic activity, as evidenced by its performance. It is, thus, recommended that future research expand the simulation time beyond 100,000 fs to provide insights into the mechanisms that drive catalyst deactivation and assist in the optimization of nickel clusters for CH_4 decomposition and H_2 generation over extended periods

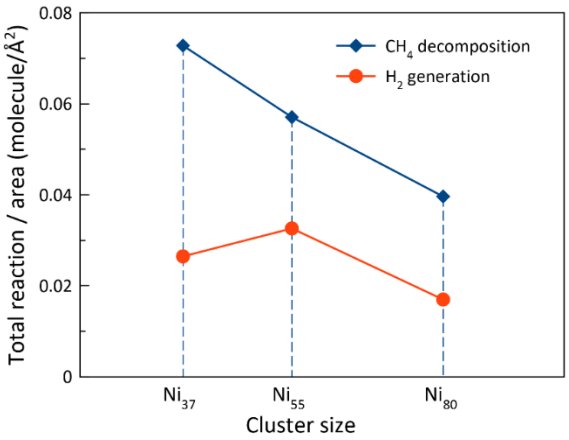

Figure 3 Calculated total reaction/surface area ratio for CH_4 decomposition and H_2 generation on Ni_{37}, Ni_{55}, and Ni_{80} clusters over 100,000 fs at T = 1,500 K.

The efficiencies of the catalysts were determined by calculating the total number of CH_4 decomposition and H_2 formation reactions per unit surface area over 100,000 fs. The system containing Ni_{37} exhibited the highest number of CH_4 decomposition events per unit of surface area during the simulation period, followed by the Ni55 system, with the Ni_{80} system displaying the lowest number (Figure 3). This suggests that smaller clusters, such as Ni_{37}, have higher surface reactivity for CH_4 decomposition at the outset.

Nevertheless, a notable outcome was observed for the formation of the H_2 molecules. As illustrated in Figure 3, the system containing the Ni_{55} nanoclusters yielded the highest number of H_2 formation reactions per unit surface area. This implies that although the Ni_{37} clusters display a higher initial reactivity for CH_4 decomposition, the Ni_{55} clusters exhibit superior efficacy as H_2 production catalysts when considering the reaction events per unit surface area.

However, it should be noted that these observations were predicted on a simulation period of 100,000 fs. Additional research is required to assess the long-term stability and efficacy of these catalysts over longer reaction times. Extended simulations can offer a more comprehensive understanding of the durability and sustained catalytic performance of Ni clusters, thereby guaranteeing the reliability of the obtained insights for real-world applications.

CH_4 Decomposition and H_2 Generation on Ni_{55} Clusters

Ni_{55} clusters were used as a model system to elucidate the processes involved in CH_4 decomposition and subsequent production of H_2. We explored the reaction pathways observed in the simulations, focusing on the complex interactions between the CH_4 molecules and the nickel cluster surface. A comprehensive analysis of the chronological order of dissociation events and subsequent formation of H_2 molecules was conducted to explain the catalytic processes involved.

DOI: 10.5614/j.eng.technol.sci.2025.57.1.5

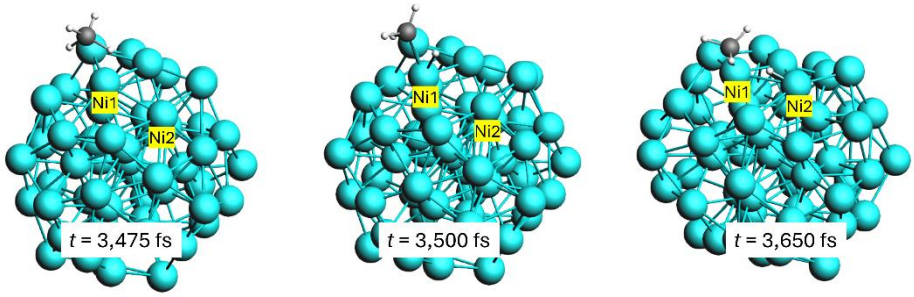

Figure 4 Snapshots showing the dissociation of a CH4 molecule on the surface of a Ni55 cluster at T = 1,500 K. The carbon atoms are shown in black, hydrogen atoms in white, and nickel atoms in cyan.

Figure 4 shows the sequence of events that occurred during CH_4 dissociation. At t = 3,475 fs, a CH_4 molecule in close proximity to a nickel atom (Ni1) can be observed on the surface of the cluster. A hydrogen atom subsequently separates from the CH_4 molecule and forms a bond with Ni1 at t = 3,500 fs. At t = 3,650 fs, a hydrogen atom migrated and formed a bond with a nickel atom (Ni2).

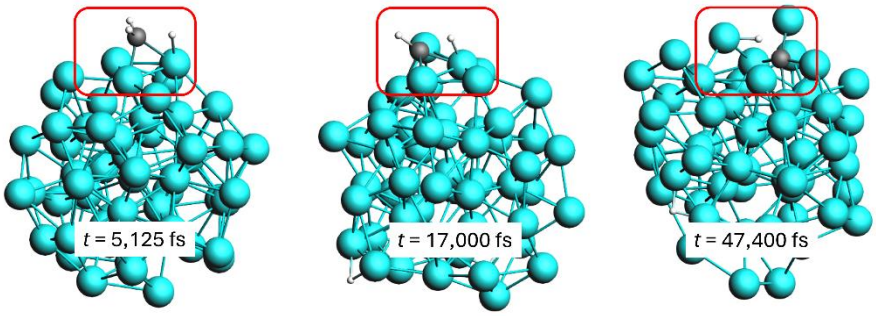

Figure 5 Snapshots showing the dissociation of methyl (left), methylene (center), and methylidyne (right) fragments on the surface of a Ni_{55} cluster at T = 1,500 K. The carbon atoms are shown in black, hydrogen atoms in white, and nickel atoms in cyan.

Figure 5 shows that the dissociation of a hydrogen atom from the CH_3 fragment occurred immediately after the initial dissociation event from the CH_4 molecule. The second dissociation of a hydrogen atom occurred at 5,125 fs, and after a considerable period, the third hydrogen atom separated from the CH_4 molecule at t = 17,000 fs, leaving behind a CH fragment. At t = 47,400 fs, the CH fragment ultimately underwent decomposition, resulting in the formation of one carbon atom and one hydrogen atom.

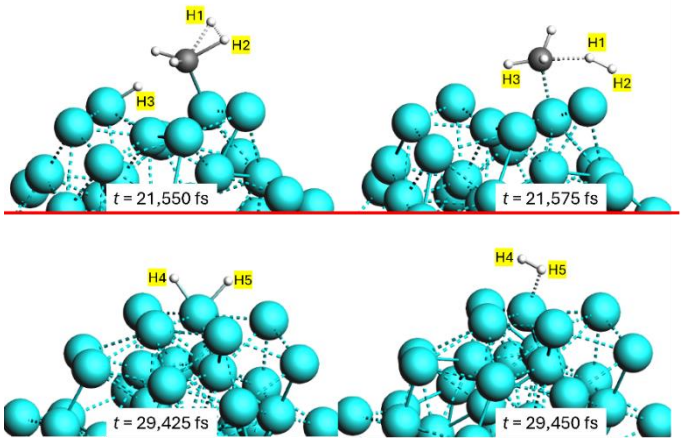

Figure 6 Snapshots showing the mechanism of H_2 molecule generation: (top) first H_2-production mechanism and (bottom) second H_2-production mechanism. The carbon atoms are shown in black, hydrogen atoms in white, and nickel atoms in cyan.

Two mechanisms for H_2 molecule formation were observed in the simulations of CH_4 reactions on Ni_{55} clusters, as shown in Figure 6. In the first mechanism (Figure 6, top), a H_2 molecule is formed when two hydrogen atoms (H1 and H2) dissociate from a CH_4 molecule in the presence of a nickel atom on the cluster surface at t = 21,550 fs. Directly after dissociation, another hydrogen atom (H3) on the nickel surface, close to the site of separation of the initial two hydrogen atoms, combines with the remaining CH_2 fragment, generating a CH_3 fragment at t = 21,575 fs. This mechanism highlights the immediate interactions and efficient rearrangement of the dissociated hydrogen atoms and CH_4 fragments on the cluster surface. In the second mechanism (Figure 6, bottom), two hydrogen atoms (H4 and H5) on the nickel cluster surface combined to form an H_2 molecule at t = 29,450 fs. This process occurs without the direct participation of CH_4 fragments, suggesting that hydrogen atoms can migrate across the surface and combine to form H_2.

The presented mechanisms demonstrate the dynamic nature of the reaction pathways on nickel clusters. The first mechanism involves the simultaneous dissociation and prompt rearrangement of hydrogen atoms and hydrocarbon fragments, resulting in the generation of H_2 and CH_3 fragments. The second mechanism illustrates the mobility of hydrogen atoms on the nickel surface, enabling them to bond and form an H_2 molecule from the original CH_4 molecule.

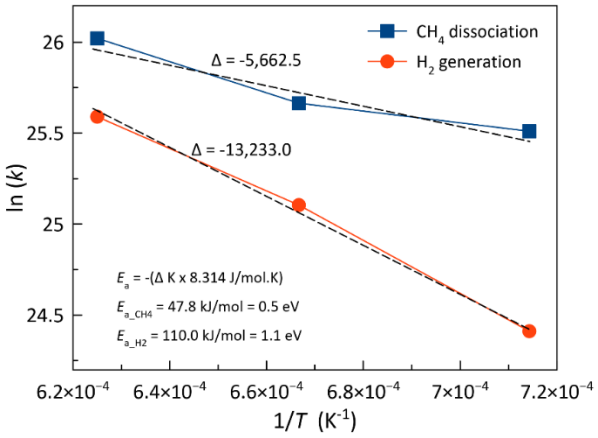

Figure 7 Plots of the natural logarithm of the reaction rate constant, ln (k), versus the reciprocal of the temperature, 1/T, for the dissociation of CH_4 molecules and H_2 generation on Ni_{55} clusters. The simulations were performed at T = 1,400 K, 1,500 K, and 1,600 K. The symbols Δ and E_a represent the slopes of the curves and activation energies, respectively.

Our present calculations indicate that the estimated activation energy for CH_4 dissociation is 0.5 eV (see Figure 7), notably lower than previously reported values on nickel surfaces (Abild-Pedersen et al., 2005; Arifin et al., 2015; Shen et al., 2016). These findings suggest that Ni clusters exhibit significantly greater reactivity than bulk Ni surfaces. The activation energy for H_2 production from CH_4 on Ni surfaces can vary depending on the specific conditions and the catalyst employed. As shown in Figure 7, the activation energy for the formation of H_2 molecules is 1.1 eV, as determined from our simulations. The substantial energy input required for H_2 production via CMD was indicated by its high activation energy. Therefore, it can be inferred that the CMD process requires a significant amount of thermal energy to overcome the energy barrier for H_2 formation.

Discussion

Molecular dynamics simulation results for CH_4 dissociation on Ni_{37}, Ni_{55}, and Ni_{80} clusters revealed that smaller nickel clusters exhibited higher reactivity. Consistently, H_2 molecules were formed earlier on the Ni_{37} cluster than on larger clusters. This finding supports those of Niu et al. (Niu et al., 2023), who used density functional theory (DFT) calculations to assess the impact of Ni cluster size on reactivity. However, despite their higher reactivity, smaller clusters such as Ni_{37} deactivate more rapidly. Therefore, the findings indicate that while smaller clusters may initially exhibit greater

DOI: 10.5614/j.eng.technol.sci.2025.57.1.5

reactivity, they are prone to faster deactivation. This is likely caused by the rapid saturation of active sites or structural modifications that decrease catalytic performance over time. Ni_{37} clusters are more susceptible to structural rearrangement and sintering because of their smaller size and higher surface energy, which results in a higher rate of deactivation. Furthermore, the increased surface-to-volume ratio of the Ni_{37} clusters enables the rapid deposition of carbon and surface poisoning, resulting in the loss of active sites. Conversely, the larger Ni_{55} and Ni_{80} clusters demonstrate a higher degree of structural stability and a reduced propensity for carbon accumulation, thereby preserving their reactivity for an extended duration.

A similar trend was observed for the production of H_2 molecules. Although the Ni_{37} cluster initially generated H_2 at a faster rate, it also underwent a precipitous decline in activity, which was comparable to its mechanism during CH_4 dissociation. In contrast, the Ni_{55} cluster maintained a higher overall yield of H_2 molecules despite its delayed initial rate compared to that of Ni_{37}. This indicates that the Ni_{55} cluster was more effective in maintaining H_2 production throughout the simulation period by maintaining a balance between reactivity and stability. The Ni_{55} clusters attain optimal equilibrium by including sufficient surface reactivity for both CH_4 decomposition and sustained H_2 production. The balanced surface properties and stability of Ni_{55} clusters are responsible for their increased efficiency because they can sustain catalytic activity throughout the simulation period. In contrast, the lower initial reactivity of the Ni_{80} clusters and swift deactivation observed in the Ni_{37} clusters restrict their overall catalytic efficacy for H_2 production within the same time frame. These findings highlight the significant potential of Ni_{55} nanoclusters as highly efficient catalysts for H_2 generation, surpassing the activities of both smaller and larger clusters in terms of reaction occurrence per unit surface area. The exceptional efficiency of the Ni_{55} clusters may prove indispensable in practical applications that require optimization of H_2 yield. Several critical structural and reactive differences can be attributed to the increased overall yield of H_2 molecules observed in the Ni_{55} cluster compared with Ni_{37} and Ni_{80}. First, the Ni_{55} clusters exhibited an optimal equilibrium between the structural stability and surface area. Compared to Ni_{37}, the Ni_{55} cluster has a greater number of active sites, which can facilitate the adsorption and dissociation of CH_4. Nevertheless, Ni_{55} has a more stable and less deformable structure, which enables it to maintain its catalytic activity over time, in contrast to Ni_{37}, which deactivates rapidly because of sintering and carbon deposition. In addition, the Ni_{55} cluster had a higher density of coordinatively unsaturated sites than Ni_{80}, which is essential for the migration and recombination of hydrogen atoms, thereby increasing the efficacy of H_2 formation. Although more stable, Ni_{80} has a lower yield of H_2 per unit surface area because it has fewer highly reactive sites in comparison to its larger size.

Analysis of the atomic trajectories obtained from the MD simulations revealed that the dissociation of CH_4 on nickel clusters proceeds in a sequential manner. After the final decomposition step, the carbon atoms were dispersed into the nickel cluster. These findings are consistent with prior research using Ni (110) (Arifin et al., 2025) and Pt_7-Ni(110) (Arifin et al., 2024) catalysts, which revealed comparable mechanisms. The sequential nature of the reaction mechanism on nickel clusters is highlighted by the stepwise dissociation of hydrogen atoms and the subsequent decomposition of the CH_4 fragment into carbon and hydrogen atoms. The rapid initial dissociation steps were followed by longer periods before further dissociation occurred, suggesting the presence of potential intermediate stabilization and energy barriers that must be overcome for the reaction to progress.

In contrast to the carbon atoms, the dissociated hydrogen atoms exhibited significant mobility on the nickel surface. This mechanism aligns with the findings of previous research, which revealed that hydrogen atoms can migrate across the nickel surface toward specific regions with low energy barriers (approximately 0.3 eV), facilitating their movement on the surface (Iskandarov & Tada, 2017). These findings emphasize the dynamic nature of the interactions of hydrogen with nickel surfaces and highlight the significance of the surface mobility in catalytic processes involving hydrogen. The efficient migration of hydrogen atoms on nickel surfaces can significantly improve the catalytic activity and stability of nickel-based catalysts in a range of applications, such as CH_4 reforming and H_2 production.

The activation energy of CH_4 dissociation on Ni surfaces has been studied extensively. According to Shen et al., the average activation barrier for CH_4 dissociation on a Ni(100) surface is approximately 0.90 eV (Shen et al., 2016), aligning with results from DFT calculations. Other researchers have also reported that the initial step of CH_4 dissociation on Ni surfaces typically represents the highest barrier, with values around 0.72–0.78 eV on Ni(111) (Arifin et al., 2015) and 0.91 eV on Ni(211) (Abild-Pedersen et al., 2005). These results were higher than the calculated activation energy of CH_4 dissociation on the Ni_{55} cluster (0.5 eV). An important aspect to consider is the change in electronic and other properties

as the size of the metal decreases from the bulk material to clusters (Rao et al., 1993). The rise in the core-level binding energy as the metal coverage decreases in clusters indicates a reduction in core-hole screening, which affects their reactivity (Rao et al., 1993). In addition, studies have documented different activation energies for CH_4 dissociation on nickel-coated surfaces. Bebelis et al. (Bebelis et al., 2000) reported activation energies ranging between 0.5 and 0.9 kcal/mol for the dissociative adsorption of CH_4 on Ni. Notably, even higher activation energies, up to 24 kcal/mol, were estimated by theoretical calculations. Zeng et al. (2021) recently reported that the apparent activation energy for the complete decomposition of CH_4 on Ni ranges from 27 kcal/mol to 30 kcal/mol. Meanwhile, Liu et al. revealed a remarkable decrease in the effective barrier for CH_4 activation, dropping from 0.9 eV on Ni(111) to a mere 0.15 eV on Ni/CeO_{2-x}(111) (Liu et al., 2016). In addition, the relationship between the catalyst and the support material can affect the activation energy. Li et al. examined the process of CH_4 synthesis from syngas on a Ce-doped Ni(111) surface. K. Li et al. identified a specific reaction pathway involving a rate-determining step with an energy barrier of 1.18 eV (K. Li et al., 2016). Further, J. Li et al. (J. Li et al., 2013) examined the impact of a metal-support interface on the dissociation of CH_4 and H_2 on $Ni/\gamma\text{-}Al_2O_3$, emphasizing the significance of this interface in the activation process. Our simulation results also indicated that the formation of H_2 molecules requires a higher activation energy than the dissociation of CH_4 on the surface of the Ni_{55} cluster catalyst.

Conclusion

MD simulations were performed using the ReaxFF force field to examine the decomposition of CH_4 and generation of H_2 on nickel clusters (Ni_{37}, Ni_{55}, and Ni_{80}). The Ni_{37} clusters exhibited the highest initial reactivity for CH_4 dissociation, although they were rapidly deactivated. In contrast, Ni_{55} and Ni_{80} maintain consistent reaction rates. The highest number of H_2 molecules per unit surface area was produced by Ni_{55} clusters within 100,000 fs, suggesting their greater efficiency in H_2 generation. The dissociation of CH_4 on the Ni55 clusters occurred sequentially. Two distinct mechanisms for H_2 formation were distinguished: simultaneous dissociation from CH_4 and migration and the combination of hydrogen atoms on the cluster surface. The activation energy for CH_4 dissociation on Ni_{55} was 0.5 eV, considerably lower than the reported values for bulk nickel, suggesting that Ni_{55} has a higher degree of reactivity. The activation energy for H_2 formation was estimated to be 1.1 eV. These findings emphasize that Ni_{55} clusters are among the most effective catalysts for CH_4 decomposition and H_2 generation because they strike a balance between structural stability and high reactivity. This combination provides new insights into the design of more effective catalytic systems for energy applications, making Ni_{55} a promising candidate for efficient CH_4 conversion and H_2 production.

Acknowledgement

This research was supported by a Fundamental Research Grant from the Ministry of Education, Culture, Research, and Technology of Indonesia, under contract number 112/VI.4/PN/2024.

Conflict of Interest Statement

The authors declare that the research was conducted without any financial or commercial relationships that could be construed as a potential conflict of interest.

References

Abild-Pedersen, F., Lytken, O., Engbæk, J., Nielsen, G., Chorkendorff, I., & Nørskov, J. K. (2005). Methane activation on Ni(111): Effects of poisons and step defects. *Surface Science, 590*(2), 127–137. https://doi.org/10.1016/j.susc.2005.05.057

Aljaradin, M. (2012). Environmental Impact of Municipal Solid Waste Landfills in Semi-Arid Climates—Case Study – Jordan. *The Open Waste Management Journal, 5*(1), 28–39. https://doi.org/10.2174/1876400201205010028

Arifin, R., Zulkarnain, Abdurrouf, Winardi, Y., Riyanto, D., & Darminto (2024). Enhanced Production of Hydrogen via Catalytic Methane Decomposition on a Pt_7-Ni (110) Substrate: A Reactive Molecular Dynamics Investigation. *Clean Energy, 8*(2), 168–176. https://doi.org/10.1093/ce/zkae017

Arifin, R., & Darminto, D. (2023). CH4dehydrogenation and H2formation on a Pt(100) Surface: An Insight From the Reactive Molecular Dynamics Simulations. *New Journal of Chemistry, 47*(24), 11444–11449. https://doi.org/10.1039/d3nj00693j

DOI: 10.5614/j.eng.technol.sci.2025.57.1.5

Arifin, R., Shibuta, Y., Shimamura, K., & Shimojo, F. (2015). First Principles Calculation of CH4 Decomposition on Nickel (111) Surface. *The European Physical Journal B, 88*(11). https://doi.org/10.1140/epjb/e2015-60557-7

Arifin, R., Winardi, Y., Zulkarnain, Abdurrouf, Darminto, Johari, N., & Selamat, A. (2025). Reactive Molecular Simulations of Catalytic Methane Decomposition on Ni (1 1 0) Surface. *Chemical Engineering & Technology, 48*(1), e202300445. https://doi.org/10.1002/ceat.202300445

Bebelis, S., Zeritis, A., Tiropani, C., & Neophytides, S. G. (2000). Intrinsic Kinetics of the Internal Steam Reforming of CH4over a Ni−YSZ−Cermet Catalyst−Electrode. *Industrial & Engineering Chemistry Research, 39*(12), 4920–4927. https://doi.org/10.1021/ie000350u

Casey, J. A., Cushing, L., Depsky, N., & Morello‐Frosch, R. (2021). Climate Justice and California's Methane Superemitters: Environmental Equity Assessment of Community Proximity and Exposure Intensity. *Environmental Science & Technology, 55*(21), 14746−14757. https://doi.org/10.1021/acs.est.1c04328

Chen, Q., & Lua, A. C. (2020). Synthesis of Electroless Ni Catalyst Supported On SBA‐15 for Hydrogen and Carbon Production by Catalytic Decomposition of Methane. *International Journal of Energy Research, 45*(2), 2810−2823. https://doi.org/10.1002/er.5975

Chenoweth, K., van Duin, A. C. T., & Goddard, W. A. (2008). ReaxFF Reactive Force Field for Molecular Dynamics Simulations of Hydrocarbon Oxidation. *The Journal of Physical Chemistry A, 112*(5), 1040–1053. https://doi.org/10.1021/jp709896w

Dipu, A. L. (2021). Methane Decomposition into Co x ‐free Hydrogen Over a Ni‐based Catalyst: An Overview. *International Journal of Energy Research, 45*(7), 9858−9877. https://doi.org/10.1002/er.6541

Doye, J. P. K., & J. Wales, D. (1998). Global minima for transition metal clusters described by Sutton–Chen potentials. New Journal of Chemistry, 22(7), 733–744. https://doi.org/10.1039/A709249K

Fujimoto, Y., & Ohba, T. (2022). Size-Dependent Catalytic Hydrogen Productionviamethane Decomposition and Aromatization at a Low-Temperature Using Co, Ni, Cu, Mo, and Ru Nanometals. *Physical Chemistry Chemical Physics, 24*(47), 28794–28803. https://doi.org/10.1039/d2cp03713k

Gallego-Villada, L. A., Perez-Sena, W. Y., Sánchez-Velandia, J. E., Cueto, J., del Mar Alonso-Doncel, M., Wärmå, J., Mäki-Arvela, P., Alarcón, E. A., Serrano, D. P., & Murzin, D. Yu. (2024). Synthesis of dihydrocarvone over dendritic ZSM-5 Zeolite: A comprehensive study of experimental, kinetics, and computational insights. *Chemical Engineering Journal, 498*, 155377. https://doi.org/10.1016/j.cej.2024.155377

Gamal, A., Eid, K., Kumar, D., & Kumar, A. (2021). Catalytic Methane Decomposition to Carbon Nanostructures and COx-Free Hydrogen: A Mini-Review. *Nanomaterials, 11*(5), 1226. https://doi.org/10.3390/nano11051226

Harbin, H., Unruh, D. K., Casadonte, D. J., & Khatib, S. J. (2023). Sonochemically Prepared Ni-Based Perovskites as Active and Stable Catalysts for Production of COx-Free Hydrogen and Structured Carbon. *ACS Catalysis, 13*(7), 4205–4220. https://doi.org/10.1021/acscatal.2c05672

Harrath, K., Yao, Z., Jiang, Y., Wang, Y., & Li, J. (2023). Activity Origin of the Nickel Cluster on TiC Support for Nonoxidative Methane Conversion. *The Journal of Physical Chemistry Letters, 14*(17), 4033–4041. https://doi.org/10.1021/acs.jpclett.3c00375

Hasnan, N. S. N., Pudukudy, M., Yaakob, Z., Kamarudin, N. H. N., Lim, K. L., & Timmiati, S. N. (2023). Promoting Effects of Copper and Iron on Ni/MSN Catalysts for Methane Decomposition. *Catalysts, 13*(7), 1067. https://doi.org/10.3390/catal13071067

Hasnan, N. S. N., Timmiati, S. N., Lim, K. L., Yaakob, Z., Kamaruddin, N. H. N., & Teh, L. P. (2020). Recent Developments in Methane Decomposition Over Heterogeneous Catalysts: An Overview. *Materials for Renewable and Sustainable Energy, 9*(2). https://doi.org/10.1007/s40243-020-00167-5

Iskandarov, A., & Tada, T. (2017). First-Principles Study of Dopant Effect on Hydrogen Oxidation in Anode of Solid Oxide Fuel Cell. *ECS Transactions, 78*(1), 1469–1475. https://doi.org/10.1149/07801.1469ecst

Kikuchi, R. (2002). Views on Methane Hydrate for Zero-Emission Energy. *Energy & Environment, 13*(1), 105–113. https://doi.org/10.1260/0958305021501100

Li, J., Croiset, E., & Ricardez‐Sandoval, L. A. (2013). Effect of Metal−Support Interface During CH4and H2Dissociation on Ni/Γ-Al2O3: A Density Functional Theory Study. *The Journal of Physical Chemistry C, 117*(33), 16907−16920. https://doi.org/10.1021/jp402421q

Li, K., Yin, C., Zheng, Y., He, F., Wang, Y., Jiao, M., & Tang, H. (2016). DFT Study on the Methane Synthesis From Syngas on a Cerium-Doped Ni(111) Surface. *The Journal of Physical Chemistry C, 120*(40), 23030–23043. https://doi.org/10.1021/acs.jpcc.6b07400

Liang, W., Chen, C., Dong, L., Tan, K., Feng, X., Liu, Y., Chen, X., Yang, C., & Shan, H. (2020). Revealing the Effect of Nickel Particle Size on Carbon Formation Type in the Methane Decomposition Reaction. *Catalysts, 10*(8), 890. https://doi.org/10.3390/catal10080890

Liu, Z., Grinter, D. C., Lustemberg, P. G., Nguyen‐Phan, T., Zhou, Y., Luo, S., Waluyo, I., Crumlin, E. J., Stacchiola, D., Zhou, J., Carrasco, J., Busnengo, H. F., Ganduglia‐Pirovano, M. V., Senanayake, S. D., & Rodríguez, J. A. (2016). Dry Reforming of Methane on a Highly‐Active Ni‐CeO2 Catalyst: Effects of Metal‐Support Interactions on C−H Bond Breaking. *Angewandte Chemie, 55*(26), 7455–7459. https://doi.org/10.1002/anie.201602489

Lu, X. (2021). Study on Comprehensive Utilization Technology of Low Concentration Coal Bed Methane. *E3s Web of Conferences, 290*, 03010. https://doi.org/10.1051/e3sconf/202129003010

Mueller, J. E., van Duin, A. C. T., & Goddard, W. A. I. (2010). Development and Validation of ReaxFF Reactive Force Field for Hydrocarbon Chemistry Catalyzed by Nickel. *The Journal of Physical Chemistry C, 114*(11), 4939–4949. https://doi.org/10.1021/jp9035056

Niu, J., Zhang, C., Liu, H., Jin, Y., Zhang, R., & Ran, J. (2023). Unraveling the effects of Ni particle size and facet on CH4 activation: From cluster to nanoparticle. *International Journal of Hydrogen Energy, 48*(51), 19486–19493. https://doi.org/10.1016/j.ijhydene.2023.02.044

Phichairatanaphong, O., Teepakakorn, P., Poo‐arporn, Y., Chareonpanich, M., & Donphai, W. (2021). Infiltrate Mesoporous Silica-Aluminosilicate Structure Improves Hydrogen Production via Methane Decomposition Over a Nickel-Based Catalyst. *Industrial & Engineering Chemistry Research, 60*(12), 4562–4574. https://doi.org/10.1021/acs.iecr.0c06355

Rad, L. F., Amini, M. R., Ahmadi, A., & Hoseinzadeh, S. (2022). Environmental and Economic Assessments of Hydrogen Utilization in the Transportation Sector of Iran. *Chemical Engineering & Technology, 46*(3), 435–446. https://doi.org/10.1002/ceat.202100500

Rao, C. N. R., Vijayakrishnan, V., Aiyer, H. N., Kulkarni, G. U., & Subbanna, G. N. (1993). An Investigation of Well-Characterized Small Gold Clusters by Photoelectron Spectroscopy, Tunneling Spectroscopy, and Cognate Techniques. The Journal of Physical Chemistry, 97(43), 11157–11160. https://doi.org/10.1021/j100145a006

Roshchanka, V., & Evans, M. (2014). Incentives for Methane Mitigation and Energy‐efficiency Improvements in the Case of Ukraine's Natural Gas Transmission System. *Earth S Future, 2*(6), 321−330. https://doi.org/10.1002/2013ef000204

Sanchez‐Bastardo, N., Schlögl, R., & Ruland, H. (2021). Methane Pyrolysis for Zero-Emission Hydrogen Production: A Potential Bridge Technology From Fossil Fuels to a Renewable and Sustainable Hydrogen Economy. *Industrial & Engineering Chemistry Research, 60*(32), 11855–11881. https://doi.org/10.1021/acs.iecr.1c01679

Santos, J. M. d., Gomes, J. G., Antônio Carlos Daltro de Freitas, & Guiradello, R. (2022). An Analysis of the Methane Cracking Process for CO2-Free Hydrogen Production Using Thermodynamic Methodologies. *Methane, 1*(4), 243–261. https://doi.org/10.3390/methane1040020

Shelepova, E. V., Maksimova, T. A., Bauman, Y. I., Mishakov, I. V., & Vedyagin, A. A. (2022). Experimental and Simulation Study on Coproduction of Hydrogen and Carbon Nanomaterials by Catalytic Decomposition of Methane-Hydrogen Mixtures. *Hydrogen, 3*(4), 450–462. https://doi.org/10.3390/hydrogen3040028

Shen, X., Zhang, Z., & Zhang, D. H. (2016). Eight-Dimensional Quantum Dynamics Study of CH4 and CD4 Dissociation on Ni(100) Surface. *The Journal of Physical Chemistry C, 120*(36), 20199–20205. https://doi.org/10.1021/acs.jpcc.6b07265

Strizhenok, A. V., & Korelskiy, D. S. (2019). Estimation and Reduction of Methane Emissions at the Scheduled and Repair Outages of Gas-Compressor Units. *Journal of Ecological Engineering, 20*(1), 46–51. https://doi.org/10.12911/22998993/93943

Stukowski, A. (2009). Visualization and analysis of atomistic simulation data with OVITO–the Open Visualization Tool. *Modelling and Simulation in Materials Science and Engineering, 18*(1), 015012. https://doi.org/10.1088/0965-0393/18/1/015012

Sun, Z. (2024). Reinforcing Hydrogen and Carbon Nanotube Coproduction via Cr–O–Ni Catalyzed Methane Decomposition. *Journal of Materials Chemistry A, 12*(8), 4893–4902. https://doi.org/10.1039/d3ta06921d

van Duin, A. C. T., Dasgupta, S., Lorant, F., & Goddard, W. A. (2001). ReaxFF: A Reactive Force Field for Hydrocarbons. *The Journal of Physical Chemistry A, 105*(41), 9396–9409. https://doi.org/10.1021/jp004368u

van Duin, A. C. T., W.A. Goddard, M.M. Islam, van Schoot, H., T. Trnka, & A.L. Yakovlev. (n.d.). ReaxFF 2024.1 (Version 2024.1) [Computer software]. SCM. http://www.scm.com

Vlaskin, M. S. (2023). Thermal Decomposition of Methane in Capillary Tubes of Different Materials: Corundum, Titanium, Nickel, and Stainless Steel. *Applied Sciences, 13*(23), 12663. https://doi.org/10.3390/app132312663

DOI: 10.5614/j.eng.technol.sci.2025.57.1.5

Wang, H. Y., & Lua, A. C. (2012). Development of Metallic Nickel Nanoparticle Catalyst for the Decomposition of Methane Into Hydrogen and Carbon Nanofibers. *The Journal of Physical Chemistry C, 116*(51), 26765–26775. https://doi.org/10.1021/jp306519t

Wang, P., Wang, S., Lin, R.-B., Mou, X., & Ding, Y. (2021). Pre-Coking Strategy Strengthening Stability Performance of Supported Nickel Catalysts in Chloronitrobenzene Hydrogenation. *Catalysts, 11*(10), 1156. https://doi.org/10.3390/catal11101156

Yan, Q., Ketelboeter, T., & Cai, Z. (2022). Production of COx-Free Hydrogen and Few-Layer Graphene Nanoplatelets by Catalytic Decomposition of Methane Over Ni-Lignin-Derived Nanoparticles. *Molecules, 27*(2), 503. https://doi.org/10.3390/molecules27020503

Zeng, J., Tarazkar, M., Palmer, C., Gordon, M. J., Metiu, H., & McFarland, E. W. (2021). Initial Steps in CH4 Pyrolysis on Cu and Ni. *The Journal of Physical Chemistry C, 125*(34), 18665–18672. https://doi.org/10.1021/acs.jpcc.1c03606

Zhang, P., Yang, Y., Duan, X., Liu, Y., & Wang, S. (2021). Density Functional Theory Calculations for Insight into the Heterocatalyst Reactivity and Mechanism in Persulfate-Based Advanced Oxidation Reactions. *ACS Catalysis, 11*(17), 11129–11159. https://doi.org/10.1021/acscatal.1c03099

Manuscript Received: 12 August 2024
Revised Manuscript Received: 16 November 2024
Accepted Manuscript: 9 January 2024